Materials and Design 120 (2017) 298–306

Contents lists available at ScienceDirect

Materials and Design

journal homepage: www.elsevier.com/locate/matdes

Influence of a sputtered compact TiO_2 layer on the properties of TiO_2 nanotube photoanodes for solid-state DSSCs

A. Krumpmann[a,*], J. Dervaux[b], L. Derue[c], O. Douhéret[c], R. Lazzaroni[c,d], R. Snyders[b], A. Decroly[a]

[a] Service de Science des Matériaux, Université de Mons, Rue de l'Epargne 56, Mons 7000, Belgium
[b] Chimie des Interactions Plasma Surface, CIRMAP, Université de Mons, 23 Place du Parc, Mons B7000, Belgium
[c] Chimie des Matériaux Nouveaux, Materia Nova Research Center, Avenue Copernic 1, Mons 7000, Belgium
[d] Chimie des Matériaux Nouveaux, CIRMAP, Université de Mons, 23 Place du Parc, Mons B7000, Belgium

HIGHLIGHTS

- A sputtered TiO_2 underlayer limits the side reaction of water oxidation during anodization, suppressing delamination issues of TiO_2 nanotubes layers.
- The complete oxidation of titanium leads to an increased average transmittance in the visible from 65% to 74%.
- The electrical conductivity of the photoelectrodes with the underlayer is increased by an order of magnitude.
- The compact underlayer leads to an improved efficiency of these solid-state dye-sensitized solar cells, from 1.0% to 1.6%.

GRAPHICAL ABSTRACT

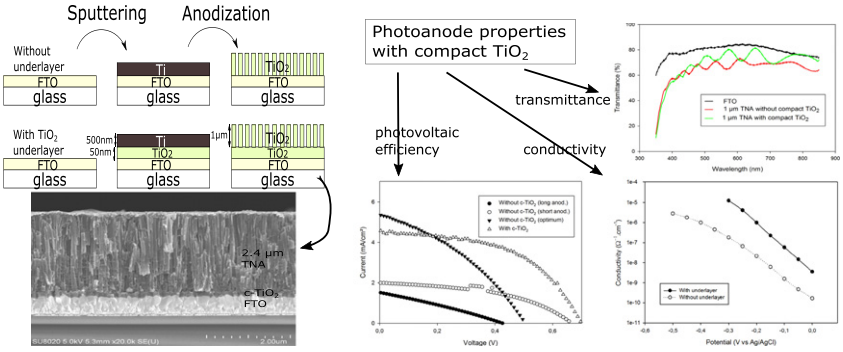

ARTICLE INFO

Article history:
Received 7 November 2016
Received in revised form 8 February 2017
Accepted 9 February 2017
Available online 12 February 2017

Keywords:
Dye solar cells
Nanotubes
Thin films
Sputtering
Anodization

ABSTRACT

TiO_2 nanotube arrays (TNA) elaborated on transparent and conducting substrates are promising materials for photoanodes in dye-sensitized solar cells as the reduced dimensionality enhances their transport properties. TNA were obtained by anodization of Ti films deposited by magnetron sputtering on transparent conducting oxide-coated glass. This study presents the impact of introducing a compact TiO_2 underlayer on the morphological, optical and electrochemical properties of the TNA photoanodes.

The TNA morphology was found to be more regular with a TiO_2 underlayer and the macroscopic homogeneity of the samples was also increased. This is ascribed to a strong reduction, in the presence of the compact TiO_2 underlayer, of a side reaction leading to oxygen evolution and destructuring the TNA film during anodization.

As a consequence, the optical and transport properties (characterized by UV–vis and electrochemical impedance spectroscopy, respectively) were improved, together with an increased photovoltaic efficiency.

* Corresponding author.
E-mail address: arnaud.krumpmann@umons.ac.be (A. Krumpmann).

http://dx.doi.org/10.1016/j.matdes.2017.02.028
0264-1275/

1. Introduction

Recently, considerable efforts have been made to develop solar cell technologies that use low-cost and non-toxic materials while being highly efficient. Among these technologies, dye-sensitized solar cells [1] (DSSC) and hybrid (organic–inorganic) solar cells [2] (HSC) are excellent candidates, which commonly use mesoporous titanium dioxide as an n-type semiconductor to make photoanodes, especially 3-D networks of 10–20 nm nanoparticles.

However, as pointed out in a recent review [3], elaborating nanostructured electrodes with a preferential dimension for electron transport (commonly called 1-D nanostructures), such as nanotubes [4], nanorods [5,6] and nanowires [7], is a further promising strategy to improve the performance of those devices. Those structures present a more direct transport pathway to the current-collecting electrode without interparticle connections [8], thus increasing the electron diffusion length [9], but they also allow a better infiltration of the organic components in HSC or solid-state DSSC [10] due to the less intricate shape of the nanostructure. Because of these advantages, 1-D TiO_2 nanostructures are good candidates for a wide range of applications, such as photocatalysis [11], hydrogen production [12], gas sensors [13] and supercapacitors [14].

In this context, the anodization of titanium in fluoride-containing electrolytes in order to obtain titania nanotube arrays (TNAs) has been extensively studied [15–17] because it is a simple and cost-effective method to obtain a nanotubular structure with a precise control of the structure, in particular the TiO_2 nanotube length and diameter.

The anodization is most commonly performed on titanium foils, which leads to a TiO_2 film on an opaque Ti substrate which can be used as an electrode in DSSCs only if illumination takes place through the counter electrode. This strategy has been used for liquid-state [18] or gel-state [19] DSSCs with a platinized fluorine-doped tin oxide (FTO) glass counter electrode, but not for solid-state cells in which a metallic (Ag or Au) counter electrode causes strong absorption losses. This can be avoided by using TNA on a transparent and conducting substrate such as FTO-coated glass.

TNA on FTO glass can be obtained by transferring a TNA deposit, previously grown on a Ti foil, onto an FTO substrate [20,21] but this method can hardly be scaled up to industrial dimensions and quantities and also seems more appropriate for long nanotubes, i.e. for liquid-state cells. Another way is to grow the TNA directly on FTO by anodizing a Ti thin film previously deposited by sputtering [22–24]. In this case, the anodization is performed until the transparency of the film is obtained, indicating full conversion of the Ti into TiO_2. However, the substrate on which the anodization is performed has an influence on the properties of the TNA film, especially because of interactions with the electrolyte at the end of the process. Therefore, an alternative method is to first deposit a compact TiO_2 underlayer by reactive magnetron sputtering of a Ti target in the presence of oxygen and then stop the oxygen flow to grow the metallic Ti layer. These methods are schematized in Fig. 1. It should be mentioned that a compact TiO_2 underlayer can also act as a blocking layer in the solar cell, even if blocking layers deposited by reactive sputtering may not be as efficient as those prepared by spray pyrolysis in classical DSSCs [25,26]. This paper aims at understanding the impact of introducing a compact TiO_2 underlayer on the morphological, optical and electrochemical properties of TNA as well as the result on the efficiency of solid-state DSSCs.

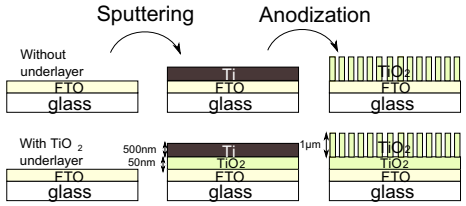

Fig. 1. Two methods to grow TNA on FTO glass: With and without TiO_2 underlayer.

2. Method

2.1. Elaboration of TiO_2 nanotube arrays on FTO glass

Reactive magnetron sputtering experiments were carried out in a cylindrical stainless steel chamber (height: 60 cm, diameter: 42 cm). The chamber was evacuated by a turbo-molecular pump (*Edwards* nEXT400D 160 W), backed by a dry primary pump, down to a residual pressure of 10^{-4} Pa. An unbalanced magnetron cathode was installed at the top of the chamber facing the substrate at a distance of 80 mm. A 2-inch diameter and 0.25-inch thick Ti target (99.99% purity) was used. The target was sputtered in DC mode using an Advanced Energy MDK 1.5 K power supply [27]. A mixture of argon (8 sccm) and oxygen (2 sccm) was injected into the chamber in order to grow stoichiometric TiO_2 film (poisoned regime) as a compact layer (50–100 nm) whereas, in the second step, the oxygen flow was stopped to grow the metallic Ti layer (500 nm or 1 µm). FTO-coated glass was used as the substrate, cleaned with a detergent (RBS) solution and rinsed with ultra-pure water. The total pressure and the sputtering power were kept constant at 0.1 Pa and 150 W, respectively. When no compact TiO_2 layer was used, the substrates were heated to 450 °C to ensure good adhesion of the film.

The Ti films were converted into TiO_2 films by anodic oxidation in an ethylene glycol solution (99.5%, *Merck*) containing 0.3 wt% NH_4F and 2 wt% water. A two-electrode configuration was used for the anodization, with a platinum foil as cathode. The anodization was carried out at a constant potential (applied by a DC power source *TTi* CPX200, Dual 35 V-10 A) at room temperature. The distance between the two electrodes was 3 cm. The anodization was performed until the transparency of the film was achieved. The anodized samples were rinsed with deionized water and then crystallized by annealing at 450 °C in air for 2 h with a heating ramp of 5 °C min^{-1} in a *Nabertherm* LT 15/12 furnace.

2.2. Characterization

The crystal structure of TNA on FTO was characterized by a *Siemens* D5000 X-ray $\theta - \theta$ diffractometer with a Co K_α ($\lambda = 0.1793$ nm) source ranging from 20 to 80°. The morphology of the titania nanotubes was studied using a field emission gun scanning electron microscope (FEG-SEM *Hitachi* SU8020).

UV–vis measurements were performed using an integrating sphere (*Labsphere* model RSA-PE-19) attached to a *Perkin Elmer* Lambda 19 UV/VIS/NIR spectrophotometer.

The electrochemical impedance spectra (EIS) were measured by using a combined potentiostat and frequency response analyzer (*Parstat* 2273 from *Ametek*). The measurements were recorded over a frequency range of 10^5 Hz to 2.10^{-2} Hz with an AC amplitude of 5 mV rms. A three-electrode cell was used in the electrochemical experiments, in which a platinum grid worked as the counter electrode and a saturated Ag/AgCl/KCl electrode as the reference. Impedance measurements were made in an NaCl 0.1 M electrolyte between 0.1 and −0.7 V vs an Ag/AgCl reference electrode. The active area of the samples was 1 cm^2. The electrochemical parameters were obtained by fitting with an electric equivalent circuit using the *ZView* software.

2.3. Solid-state DSSC fabrication and testing

The dye impregnation of the TNA photoelectrodes was performed in a 0.1 mM C106 dye (*Dyesol*) solution (the solvent being a 1:1 mixture of acetonitrile and tert-butanol) during 18 h. After rinsing the samples with acetonitrile and drying, infiltration of the hole transport material was performed by a 30 s spin-coating at 1000 rpm after waiting 30 s to let the solution infiltrate the TNA layer. The solution was composed of spiro-OMeTAD (170 mg/ml), 4-tert-butylpyridine (20 mg/ml) and bis(trifluoromethane)sulfonimide lithium salt (Li TFSI, 16 mg/ml) in chlorobenzene. Finally, a 150 nm thick Ag counter electrode was evaporated to complete the cells that were stored 3 days under ambient conditions before testing. Solar cells testing was performed under a 1 sun illumination provided by an *ABET* solar simulator equipped with an AM 1.5 filter and calibrated with a reference silicon solar cell. The I–V characteristics of the devices were recorded using a computer-controlled *Keithley 2400*. The active area of the cells was 0.28 cm^2.

3. Results and discussion

3.1. Crystal structure and morphology

Fig. 2 shows the X-ray diffractograms of TNA on FTO glass before and after thermal treatment. The only peaks present before annealing are those of the FTO layer, which implies an amorphous TiO_2 structure. The annealing treatment at 450 °C allows crystallizing the TiO_2 in its anatase polymorph. No rutile phase is observed. In addition to crystallization, this thermal treatment allows converting the remaining titanium that would not have been oxidized by the anodization process.

Concerning the plasma deposition of Ti films directly on FTO glass, it has been reported that preheating the substrate was necessary to get a sufficient adhesion of the film, otherwise the Ti film was found to peel off when immersed in the electrolyte [28]. Another method to improve adhesion consists in applying a bias to the substrate during sputtering [23]. This problem of adhesion when no preheating or bias was applied was also observed in this work, but only for the deposition of Ti without a TiO_2 underlayer. Sufficient adhesion was obtained in all cases when a 50–100 nm TiO_2 compact underlayer was previously deposited. Therefore, the samples with a TiO_2 underlayer were made without preheating step. This improvement of the adhesion probably comes from the high energy needed to ensure a good compactness of the TiO_2 layer. By using a low pressure in the plasma chamber, a high energy plasma is created and therefore a very compact film is obtained. The drawback of this low pressure deposition is a much lower deposition rate (depositing 100 nm of compact TiO_2 requires as much time as 1 μm of the metal). The underlayer thickness of 50–100 nm was chosen as the most suitable: a minimum of 50 nm was decided to ensure a homogeneous and complete coverage of the substrate and compact layers thicker than 150 nm lead to charge extraction limitations in the solar cells. However, in the range of 50–100 nm, the properties were all found to be stable. FEG-SEM images of TNA are shown in Fig. 3 for the samples prepared (a) without and (b) with an underlayer. The morphology is similar, the only difference is a flat top layer that is observed when an underlayer is used, which makes the tubes walls seem thicker. That top layer can be avoided by a post-treatment like ultrasonication [29]. Nevertheless, having this kind of flat top layer is not a problem as long as the tubes end remains open (i.e. the dye and HTM can still penetrate in the nanotubes) and therefore the elimination of the top layer by ultrasonication had no influence on the properties of the photoelectrodes.

A cross-section view of the TNA (with a TiO_2 underlayer) is given in Fig. 4. One can clearly see the nanotubular structure, the thin compact layer, and the FTO substrate. The TNA film thickness is linked to the Ti film thickness and the anodization parameters: it varies between 1 and 2.5 μm (starting from 500 nm or 1 μm of Ti) which is consistent with studies on the expansion factor of TiO_2 nanotubes [30]. The cross-section views of TNAs without an underlayer are very similar, except for the top layer.

As is shown in Fig. 5, a smaller nanotube diameter is observed at lower voltages, the average values being approximately 30 nm at 20 V, 45 nm at 30 V, and 60 nm at 40 V. For these FEG-SEM measurements the top layer was eliminated by ultrasonication to better distinguish the nanotubular structure. This is consistent with the linear evolution of the tube diameter with the applied potential that has been reported for anodization on Ti foils [31], even if the diameter values are slightly lower in the present case. This can be ascribed to the thicker nanotube walls that come from the shortness of the tubes. The pore wall thinning effect observed for longer nanotubes [32] is reduced here; hence a smaller inner diameter is observed.

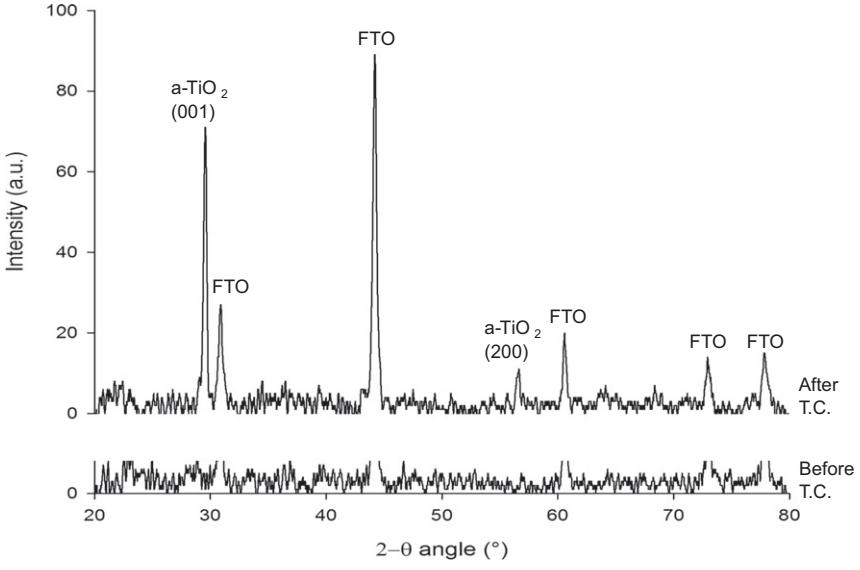

Fig. 2. XRD of TNA before and after thermal crystallization (T.C.) at 450 ° C. The a-TiO_2 label stands for anatase.

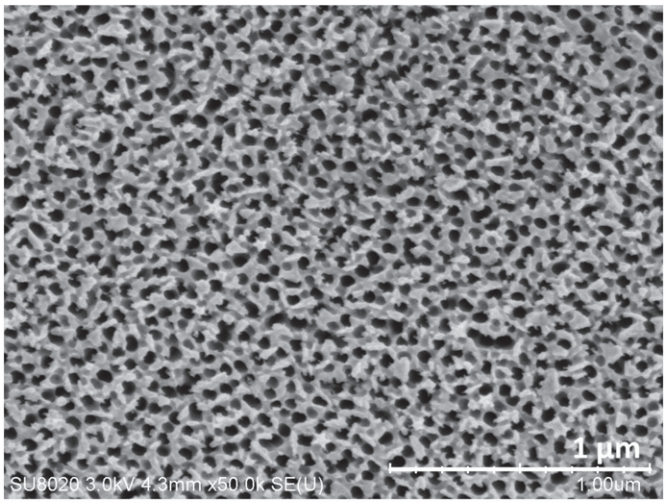

(a)

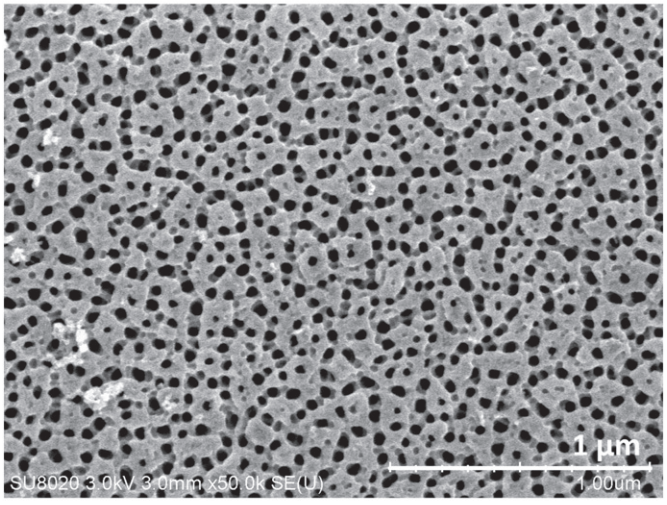

(b)

Fig. 3. FEG-SEM images of TNA (a) without and (b) with a compact TiO_2 underlayer obtained at an anodization potential of 40 V.

From a macroscopic point of view, the samples prepared using a TiO_2 underlayer are found to be more homogeneous. Images of samples made with and without an underlayer are shown in Fig. 6. Slight differences of color can be seen and a delamination of the TNA layer can occur at some places. If performed without an underlayer, the anodization has to be stopped before complete transparency is achieved in order to avoid delamination problems. The remaining titanium is converted into TiO_2 during the thermal treatment. This is not necessary for samples with a TiO_2 underlayer, as delamination is not a problem. To explain this difference in behavior, the anodization mechanism has to be described. It has been extensively studied for TiO_2 in the last decade [15,16]. At the anode, the main reaction is titanium oxidation which leads to the formation of TiO_2:

$$Ti \rightarrow Ti^{4+} + 4e^- \quad (1)$$

$$Ti^{4+} + 2H_2O \rightarrow TiO_2 + 4H^+. \quad (2)$$

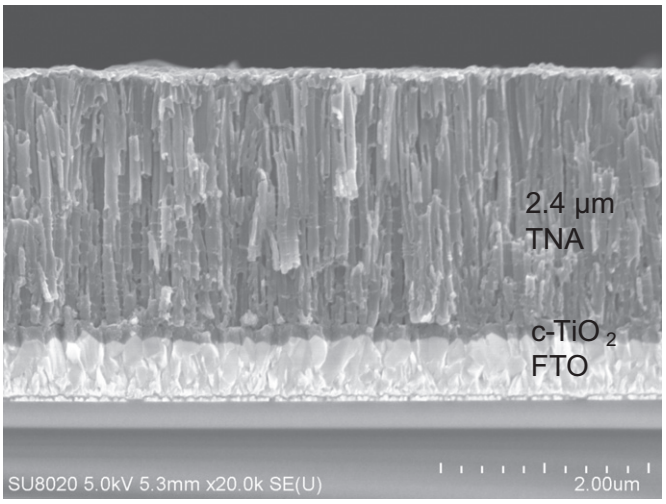

Fig. 4. Cross-section view of TNA. The Ti film was anodized at 40 V with a TiO_2 underlayer.

In the meantime, fluoride ions dissolve the oxide by forming a complex.

$$TiO_2 + 6F^- + 4H^+ \rightarrow TiF_6^{2-} + 2H_2O. \quad (3)$$

The competition between the formation of TiO_2 and its dissolution by fluoride species is known to be responsible for the nanotubular structure. However, water oxidation can take place as an anodic side reaction, leading to oxygen evolution:

$$2H_2O \rightarrow O_2 + 4H^+ + 4e^-. \quad (4)$$

This reaction could be responsible for the delamination and inhomogeneity problems. In most cases this reaction is negligible (at least in organic electrolytes with a low amount of water) because the oxidation of titanium prevails. But at the end of the anodization process, when the electrolyte is in contact with a highly conducting substrate such as FTO, the intense formation of oxygen bubbles could provoke a delamination of the TNA layer, as observed in samples anodized without an underlayer (see Fig. 7). This is consistent with: (i) the observed presence of bubbles only at the end of the anodization, (ii) the higher current recorded when approaching complete transparency, (iii) the non damaged FTO layer even in the delaminated zones and (iv) the better results obtained when stopping the anodization before the complete conversion of the Ti layer (see below). Therefore, the presence of a TiO_2 underlayer probably limits this reaction, TiO_2 being less conductive than FTO or presenting a much higher overpotential for that reaction. Indeed, during anodization, both reactions (TNA growth and water oxidation) occur at the same time, but with different intensities. Their relative intensities greatly depend on the activation overpotential which is linked to the substrate. Water oxidation is already taking place on TiO_2 at the beginning of the experiment but the intensity of that reaction is much lower than Ti oxidation and essentially TNA growth can be observed. However, when the anodization ends (or in presence of a defect, or even at the edges of the sample) and a contact (even very localized) between the FTO layer and the electrolyte is established, a new pathway (less resistive and with a lower activation overpotential) is created for the current and much more intense bubbling starts. The problem with these oxygen bubbles is the local overpressure created that provoke the delamination of the film.

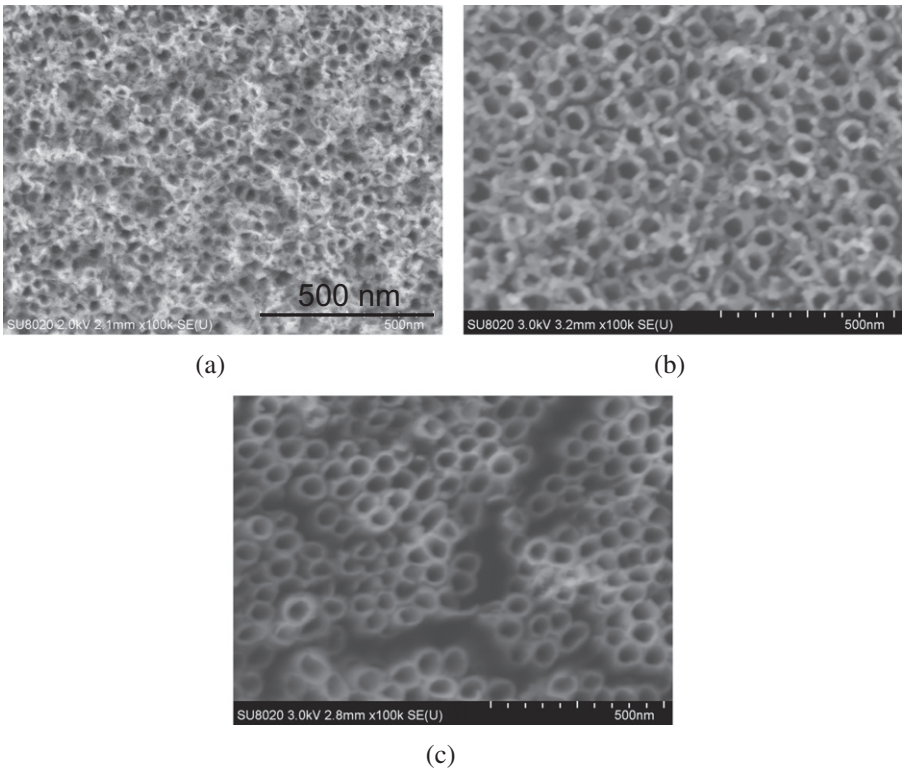

Fig. 5. FEG-SEM images of TNA anodized at (a) 20V (b) 30V (c) 40V with the same magnification. The top layer was eliminated by ultrasonication.

In order to support this explanation involving the importance of reactions at the FTO substrate during anodization, titanium was deposited on glass (without FTO layer). During the anodization of those samples, reactions can only happen between the Ti or TiO_2 and the electrolyte. In such a case, the anodization can be performed until complete transparency and no bubble is observed. Moreover, the structure obtained is free of any defect and extremely regular, as seen in Fig. 8.

Thus, introducing a compact TiO_2 layer prevents any contact between the electrolyte and the substrate, allowing the use of a highly conducting substrate (which is necessary for solar cell applications). The influence of this underlayer on the water oxidation side reaction during anodization is confirmed by evolution of the anodization current with time (Fig. 9). After a fast decrease in the first seconds (due to the formation of the oxide), the current stabilizes at about 2 mA · cm^{-2}, that is the nanotube growing regime. During that period, the two curves (with and without underlayer) are very similar (stage a in the graph). However, when the anodization proceeds further, two different behaviors are observed: in the absence of an underlayer, the current rises (stage b) due to the oxygen evolution which becomes more and more intense as the delamination takes place and the contact area between the FTO and the electrolyte increases. In the presence of an underlayer, the current decreases to almost zero (stage c), indicating the complete oxidation of the Ti without any side reaction. The anodization is stopped at that stage

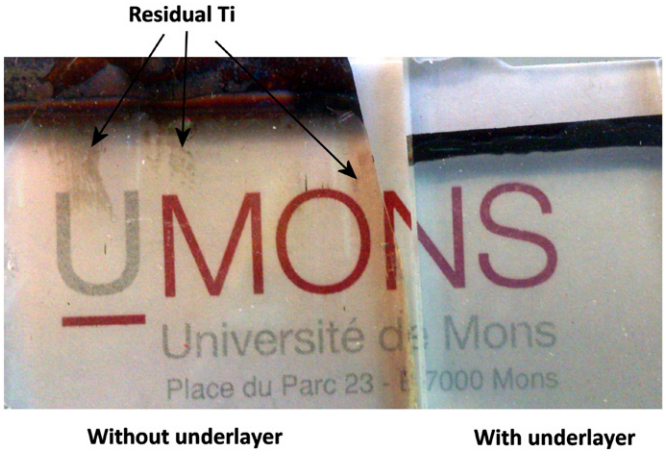

Fig. 6. Images of anodized samples after thermal treatment (right) with and (left) without a TiO_2 underlayer.

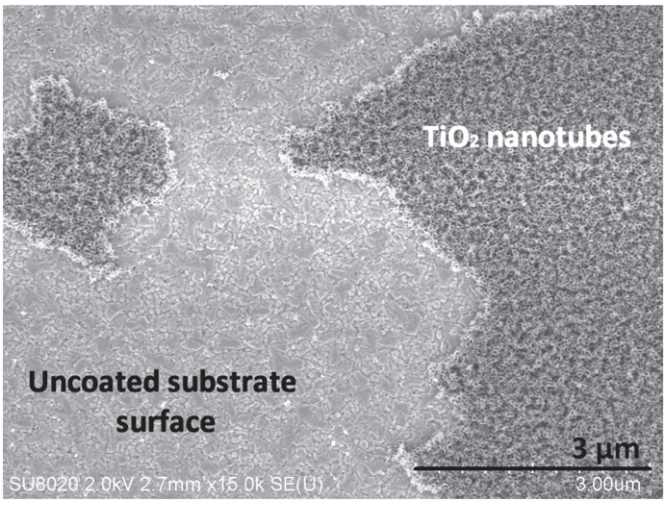

Fig. 7. FEG-SEM top view of a partially delaminated zone of the TNA layer observed on a sample without TiO_2 underlayer.

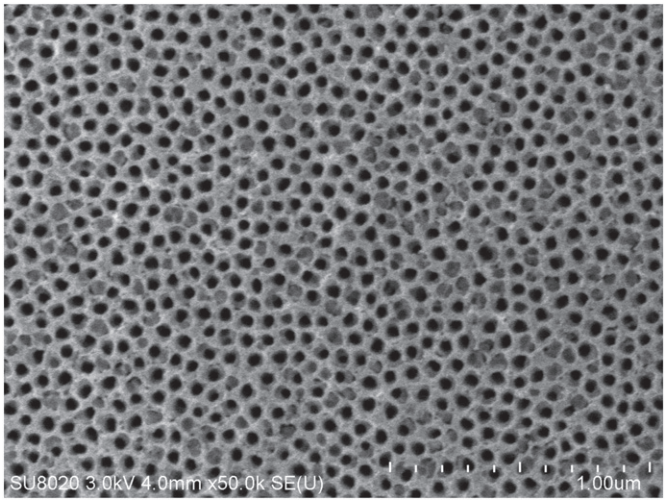

Fig. 8. FEG-SEM image of a TNA layer anodized on an insulating substrate (glass).

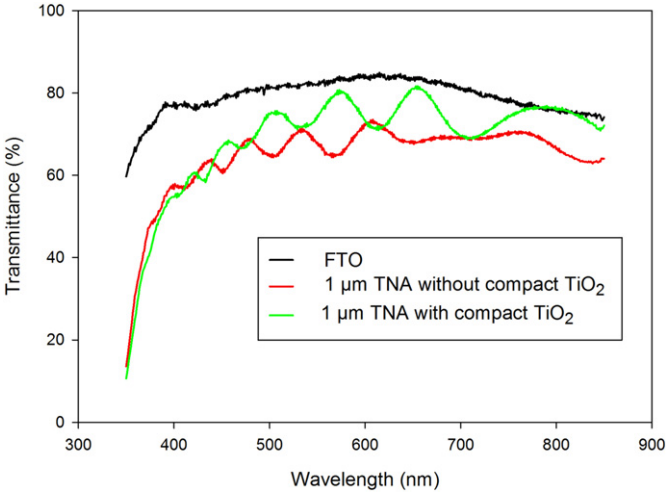

Fig. 10. Total transmitted light over the visible range for FTO substrate, TNA photoanodes with and without a TiO_2 underlayer.

because after a few minutes, the underlayer breaks, delamination can occur (stage d, often started by edge effects), and a fast increase of the current is observed, due to water oxidation.

3.2. Optical properties

The optical properties of the TNA have been characterized by UV–visible spectroscopy. A good photoanode must have the highest transmittance, including diffuse transmittance. Consequently, the optical measurements have been made using an integrating sphere. The total transmittance spectrum of the photoanodes is shown in Fig. 10. In order to compare properly the transmittance of the samples with and without a TiO_2 underlayer, the TNA thickness has to be the same for each sample. This was measured by SEM-FEG cross-sections and verified by using the envelope method [33], which allows determining the film thickness from interferences observed on the UV–vis spectrum. These optical interferences are frequently observed for transparent dielectric thin films (such as TiO_2 in the dark) and their wavelength spacing is related to the film thickness. The concordance of the values obtained with that method and the SEM measurements also identifies this phenomenon as being responsible of the wavy UV–vis spectrum. The thickness t is given by

$$t = \frac{\lambda_1.\lambda_2}{2\{\lambda_2.n(\lambda_1) - \lambda_1.n(\lambda_2)\}} \tag{5}$$

where λ_1 and λ_2 are the wavelengths associated to two adjacent minima or maxima, and $n(\lambda_1)$ and $n(\lambda_2)$ are their refractive indexes, which can be determined by the following relations:

$$n(\lambda) = \sqrt{S + \sqrt{S^2 - n_S^2}} \tag{6}$$

$$S = \frac{1}{2}n_S^2 + 2n_S\frac{T_{max} - T_{min}}{T_{max}.T_{min}} \tag{7}$$

In these equations, n_S is the refractive index of the substrate, T_{max} the maximum envelope, and T_{min} the minimum envelope. This leads to a calculated thickness of about 1.2 µm, in good accordance with FEG-SEM cross-section measurements. Due to these interferences in the UV-vis graph, only the mean value of transmittance is considered. The photoelectrodes with a TiO_2 underlayer have a high transmittance (with a mean value of about 74% between 450 and 850 nm); this is very close to the FTO transmittance, which is just over 80% in that region of the spectrum. Samples without an underlayer are less transparent (with a mean value between 63% and 68%). As the measured reflectance is similar (and very low) for both type of samples, the simple relation $A + T + R = 1$ indicates that the absorption of samples without an underlayer is higher. This was anticipated, because these films appear to be slightly coloured, most probably a result of an incomplete oxidation of Ti during the thermal annealing. The transmittance values are very reproducible when anodization fully oxidizes the titanium (i.e. for the samples with an underlayer) while it depends strongly on the amount of titanium remaining after anodization for the samples without an underlayer. This amount of residual Ti is not easily controllable, as the anodization process sometimes proceeds faster at some points of the sample (especially for large samples).

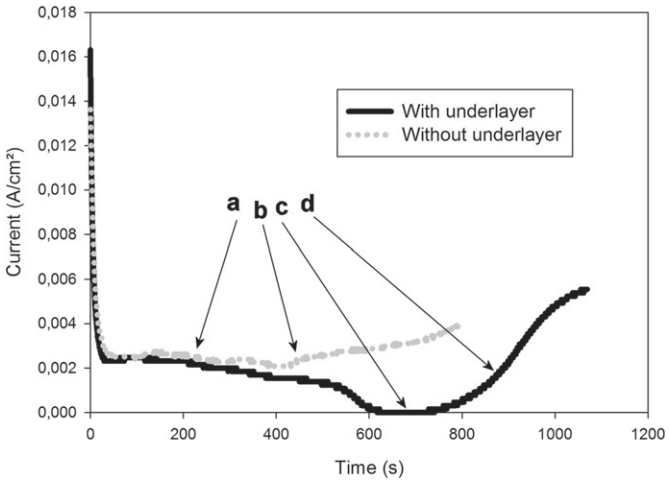

Fig. 9. Anodization current (40 V) with and without a TiO_2 underlayer, showing the importance of an underlayer for limiting the oxygen evolution side reaction.

3.3. Electrochemical characterization

Electrochemical impedance spectroscopy (EIS) has been extensively used for characterizing solar cells and very accurate models have been developed to describe the processes that take place [34].

In particular, transmission line models developed for porous electrodes [35] are of special interest for describing solar cell TiO_2 photoanodes. The model used in this paper is shown in Fig. 11 (a). It mainly consists in a transmission line distributed along the whole nanotube length (in a more general case, along the width of the sample) that takes into account the coupling between the mechanisms of charge transfer and charge transport. It contains three parameters: a parallel association of a resistance r_c and a capacitance C that models the interface between the TiO_2 layer and the electrolyte, and a resistance r_t that represents the transport resistance in the nanotubes. A typical Nyquist graph for this type of transmission line contains a high-frequency 45° line (related to r_t) along with a low-frequency semi-circle (related to r_c and C) [35]. An experimental Nyquist plot is given in Fig. 11 (b).

While r_c and C depend on both the photoanode and the electrolyte, r_t is an intrinsic property of the TiO_2 and can be easily related to the conductivity of the TNA layer which is given by [34]:

$$r_t = \sigma_n^{-1}. \tag{8}$$

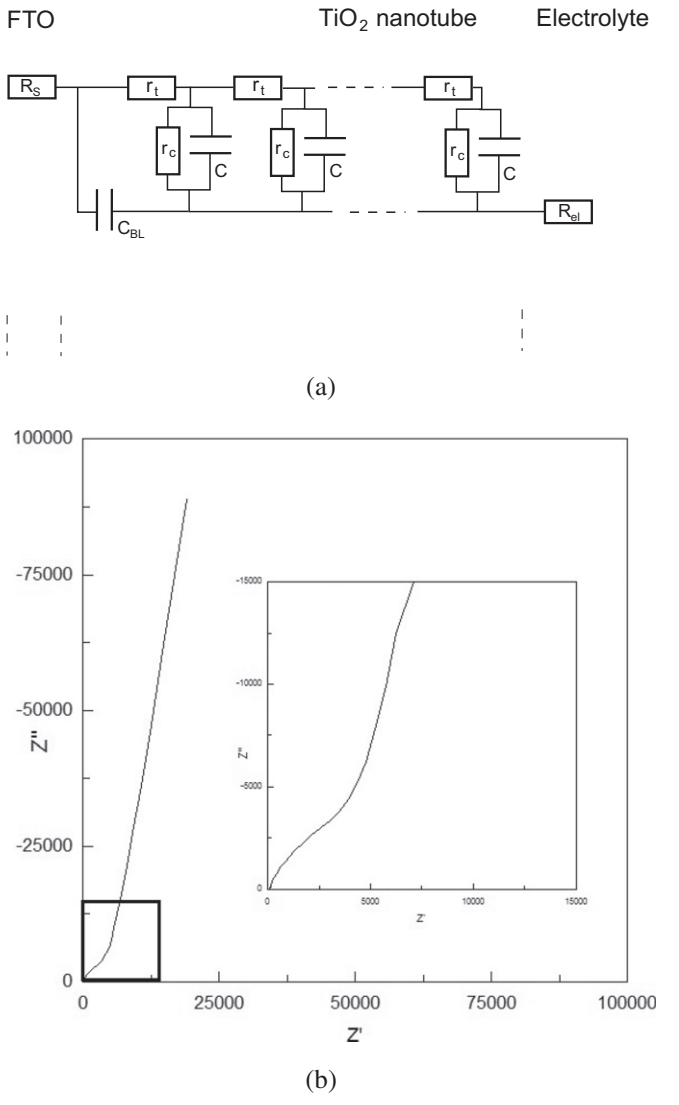

Fig. 11. (a) General model used for fitting EIS data: The parameters are R_s: series resistance, R_{el}: electrolyte resistance, r_c: charge transfer resistance, r_t: transport resistance in the TiO_2, C_{BL}, back layer capacitance and C: chemical capacitance; (b) Experimental Nyquist plot of TNA in NaCl 0.1 M at 0 V vs Ag/AgCl showing transmission line behavior. Insert is a zoom on the high frequency region representative of transport in TNA.

Measuring the transport resistance at different potentials allows a proper comparison of TiO_2 photoanode electron conductivity: modifying the applied potential induces a displacement of the Fermi level which determines the number of carriers and hence the conductivity. An exponential variation of the transport resistance is expected as the number density of carriers n_c in a semiconductor such as titanium dioxide is given by

$$n_c = N_c.e^{\frac{E_F - E_C}{k_B T}} \tag{9}$$

where N_c is the effective density of carriers, E_F the Fermi level, E_C the conduction band level, k_B Boltzmann's constant and T the temperature. Consequently, a similar exponential evolution is expected for the TiO_2 photoanode conductivity as a function of the applied potential.

It is worth noting that this method has been used to determine the conductivity of mesoporous TiO_2 yielding consistent results when compared with more classical electrical methods, assessing the reliability of the technique and models used [36]. Here, the EIS experiments were carried out in an NaCl 0.1 M aqueous electrolyte. The nature of the electrolyte is not expected to modify the values of the transport resistance as it is an intrinsic characteristic of the material, as long as the electrolyte does not modify the structure of the electrode material. For example, acidic solutions have been avoided because of electrochemical doping of the nanotubes due to proton intercalation [8].

The measured conductivities of the TNA photoanodes with and without a compact TiO_2 underlayer are shown in Fig. 12. It appears that the photoanode conductivity is at least one order of magnitude higher when a compact layer is added, over the range of potentials considered (results below −0.3 V are not given for samples with a compact layer because r_t is too small to be accurately measured). The difference is too large to be explained by the slight change of morphology of the TNA. The reason for such an increase of conductivity when using a compact layer should rather be linked to the conversion of Ti into TiO_2 . Again, introducing a TiO_2 underlayer allows a complete oxidation of Ti during anodization which is impossible without it because of oxygen evolution. In the absence of an overlayer, the remaining Ti is converted into TiO_2 by thermal treatment. This step increases the transparency and favors the crystallization of the TNA into anatase but it could lead to less conductive layers, i.e. the TiO_2 (or more exactly TiO_{2-x}) obtained by thermal treatment would be less conductive than the TNA or the sputtered compact TiO_2 layer. In order to verify this hypothesis, additional measurements have been

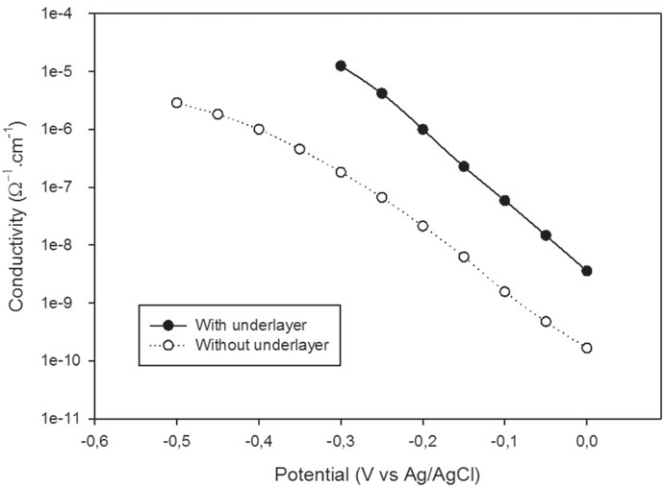

Fig. 12. Influence of a compact TiO_2 underlayer on the conductivity of TNA photoanodes as a function of the applied potential. Measured by EIS.

made on several samples from different anodization experiments. While the transport resistance of the samples with a TiO_2 underlayer is very reproducible (due to the complete oxidation of the Ti), the transport resistance of the samples without an underlayer varied by almost one order of magnitude, depending on the amount of remaining Ti, which is not easily controllable. This lower conductivity that goes with a higher remaining Ti has to be explained, as titanium is more conductive than TiO_2, and so is any well-engineered TiO_{2-x} . However, this does not mean that the whole film is more conductive for two different reasons. The first reason is that the quality of this TiO_{2-x} created due to the thermal treatment is completely uncertain: there can be defects acting as trap states, blocking the current, and the compactness of the film is certainly not as good as a plasma deposited compact layer, which also reduces the overall conductivity. The second reason is that this TiO_{2-x} introduces additional interfaces in the system and consequently additional charge transfer resistances (TNA/TiO_{2-x} and TiO_{2-x} /FTO) and these could be much more limiting than the actual conductivity of the Ti enriched layer. Using a compact underlayer thus enables obtaining the highest conductivity by a full oxidation of Ti during anodization, without destructuring the film by excessive oxygen evolution. This is of great importance, especially for obtaining homogeneous transport properties for large samples.

3.4. Solar cells performances

Solid-state DSSCs have been fabricated with those TNA photoelectrodes to determine the influence of the compact layer on the cell efficiency. 2 μm thick TNA layers have been used for this purpose, as it is considered to be an optimized thickness for solid-state DSSCs (for nanoparticles-based cells). The results are shown in Fig. 13. For the cells without compact TiO_2, anodization was stopped either just before the current increase (step (b) of Fig. 9), or just after. This strongly affects the shape of the j–V curves and the cell performances: when the anodization is stopped after the current increase has started, the efficiency is very low (0.2%) due to a very low V_{OC} (0.42 V) and FF (0.3), which can be explained by local short-circuiting due to direct access of the electrolyte to the FTO substrate, as a result of the delamination of the TNA layer induced by oxygen evolution. The opposite trend is observed when anodization is stopped before complete transparency: higher V_{OC} (0.65 V) and FF (0.52) are obtained as short-circuiting is prevented, but the drawback is the quite low J_{SC} of about 2 mA/cm^2, leading to a 0.7% efficiency. This cannot only be explained by the small loss in transparency of the TNA photoelectrode, it is essentially linked to the modification of the transport properties induced by leaving non-anodized Ti (thermally converted in TiO_2) which hampers the charge extraction. Between these two extreme behaviors, an optimum has to be found to achieve a good charge extraction while maintaining a correct diode behavior. The best cells obtained without compact layer (i.e. the anodization was stopped at optimized time, producing a homogeneous film) reached 1% efficiency (V_{OC}: 0.5 V, FF: 0.36 and J_{SC}: 5.4 mA/cm^2). This result can be compared to the cells obtained with a compact TiO_2 layer where anodization is stopped when complete transparency is achieved (at step (d) of Fig. 9). In that case, for an average cell, the J_{SC} is similar with 4.5 mA/cm^2 but the V_{OC} of 0.7 V and the FF over 0.5 are significant improvements, for an efficiency of 1.6%, i.e. a 60% increase compared to the best cells without the TiO_2 underlayer. The similar high current is consistent with the complete electrochemical oxidation of the Ti layer while the underlayer itself prevents direct contact with the FTO and thus short-circuiting, allowing this improvement of both V_{OC} and FF. In addition, the cell efficiencies are less sensitive to the anodization duration, as the anodization current drops to almost 0 during a few minutes, which means this method ensures a better reproducibility.

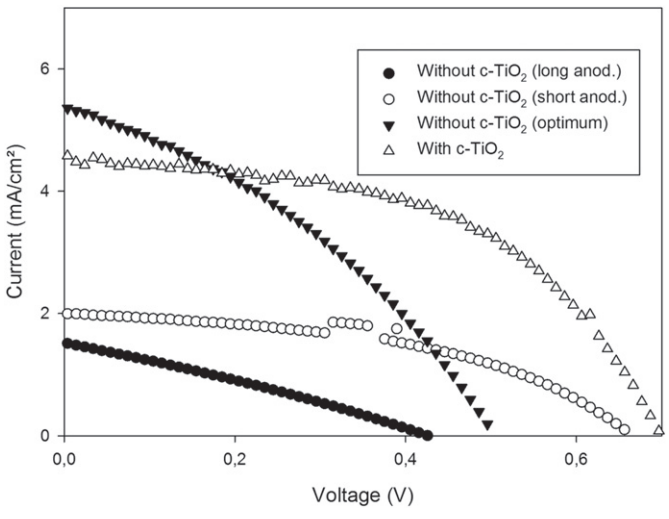

Fig. 13. j–V curves of solid-state DSSCs made with and without TiO_2 compact underlayer.

4. Conclusions

This study has shown the interest of using a compact TiO_2 underlayer for synthesizing TNA photoanodes by anodization of sputtered titanium films on FTO glass. The presence of the underlayer improves the adhesion of the Ti to the substrate but also favorably influences the properties of the system: by preventing contact between the conducting substrate and the electrolyte, it allows the complete oxidation of the titanium by anodization, creating more homogeneous layers with higher transmittance and conductivity. As a consequence, the solid-state DSSCs fabricated with a TiO_2 underlayer showed in average a 60% higher efficiency (1.6%) compared to the best cells without underlayer.

Acknowledgments

The authors would like to thank the support of the "Fédération Wallonie-Bruxelles " through the ARC project MADSSCELLS (AUWB-2012-12/17-UMONS N2). Research in Mons is also supported by the Science Policy Office of the Belgian Federal Government (IAP project 7/5) and FNRS-FRFC. A.K. also thanks the FRIA (Fonds pour la Formation à la Recherche dans l'Industrie et dans l'Agriculture) for a grant.

References

[1] B. O'Regan, M. Grätzel, A low-cost, high-efficiency solar cell based on dye-sensitized colloidal TiO_2 films, Nature 353 (1991) 737–740.
[2] M. Wright, A. Uddin, Organic-inorganic hybrid solar cells: a comparative review, Sol. Energy Mater Sol. Cells 107 (2012) 87–111.
[3] V.J. Babu, S. Vempati, S. Sundarrajan, M. Sireesha, S. Ramakrishna, Effective nanostructured morphologies for efficient hybrid solar cells, Sol. Energy 106 (2014) 1–22.
[4] P. Roy, S.P. Albu, P. Schmuki, TiO_2 nanotubes in dye-sensitized solar cells: higher efficiencies by well-defined tube tops, Electrochem. Commun. 12 (2010) 949–951.
[5] J. Luo, C. Liu, S. Yang, Y. Cao, Hybrid solar cells based on blends of poly(3-hexylthiophene) and surface dye-modified, ultrathin linear and branched TiO_2 nanorods, Sol. Energy Mater. Sol. Cells 94 (2010) 501–508.
[6] Y.-Y. Lin, T.-H. Chu, S.-S. Li, C.-H. Chuang, C.-H. Chang, W.-F. Su, C.-P. Chang, M.-W. Chu, C.-W. Chen, Interfacial nanostructuring on the performance of polymer/TiO_2 nanorod bulk heterojunction solar cells, J. Am. Chem. Soc. 131 (2009) 3644–3649.
[7] X. Feng, K. Zhu, A.J. Frank, C.A. Grimes, T.E. Mallouk, Rapid charge transport in dye-sensitized solar cells made from vertically aligned single-crystal rutile TiO_2 nanowires, Angew. Chem. 124 (2012) 2781–2784.

[8] F. Fabregat-Santiago, E.M. Barea, J. Bisquert, G.K. Mor, K. Shankar, C.A. Grimes, High carrier density and capacitance in TiO_2 nanotube arrays induced by electrochemical doping, J. Am. Chem. Soc. 130 (2008) 11312–11316.
[9] J.R. Jennings, A. Ghicov, L.M. Peter, P. Schmuki, A.B. Walker, Dye-sensitized solar cells based on oriented TiO_2 nanotube arrays: transport, trapping, and transfer of electrons, J. Am. Chem. Soc. 130 (2008) 13364–13372.
[10] H.J. Snaith, L. Schmidt-Mende, Advances in liquid-electrolyte and solid-state dye-sensitized solar cells, Adv. Mater. 19 (2007) 3189–3200.
[11] Q. Wang, Y. Xu, S. Zhang, S. Gao, Q. Zheng, Q. Yuan, W. Rong, C. Yin, J. Wang, M. Wang, Self-organized TiO_2 nanotube arrays sensitized by uniform $Cd_{0.8}Zn_{0.2}S$ nanoparticles for highly effective photoelectrochemical performance, Mater. Des. 92 (2016) 102–106.
[12] P.S. Shinde, J.W. Park, M.A. Mahadik, J. Ryu, J.H. Park, Y.-J. Yi, J.S. Jang, Fabrication of efficient CdS nanoflowers-decorated TiO_2 nanotubes array heterojunction photoanode by a novel synthetic approach for solar hydrogen production, Int. J. Hydrog. Energy 41 (2016) 21078–21087.
[13] P. Perillo, Flexible gas sensor based on TiO_2 membrane nanotubes for detection of butylamine, Mater. Today Commun. 7 (2016) 117–121.
[14] D. Ponnamma, P. Vijayan P, M.Al Ali Al-Maadeed, 3D architectures of titania nanotubes and graphene with efficient nanosynergy for supercapacitors, Mater. Des. 117 (2017) 203–212.
[15] D. Regonini, C. Bowen, A. Jaroenworaluck, R. Stevens, A review of growth mechanism, structure and crystallinity of anodized TiO_2 nanotubes, Mater. Sci. Eng., R 74 (2013) 377–406.
[16] G.K. Mor, O.K. Varghese, M. Paulose, K. Shankar, C.A. Grimes, A review on highly ordered, vertically oriented TiO_2 nanotube arrays: fabrication, material properties, and solar energy applications, Sol. Energy Mater. Sol. Cells 90 (2006) 2011–2075.
[17] N. Hu, N. Gao, Y. Chen, M.J. Starink, Achieving homogeneous anodic TiO_2 nanotube layers through grain refinement of the titanium substrate, Mater. Des. 110 (2016) 346–353.
[18] S. So, I. Hwang, P. Schmuki, Hierarchical DSSC structures based on single walled TiO_2 nanotube arrays reach backside illumination solar light conversion efficiency of 8 %, Energy Environ. Sci. 8 (2015) 849–854.
[19] Z. Seidalilir, R. Malekfar, H.-P. Wu, J.-W. Shiu, E.W.-G. Diau, High-performance and stable gel-state dye-sensitized solar cells using anodic TiO_2 nanotube arrays and polymer-based gel electrolytes, ACS Appl. Mater. Interfaces 7 (2015) 12731–12739.
[20] Q. Pang, L. Leng, L. Zhao, L. Zhou, C. Liang, Y. Lan, Dye sensitized solar cells using freestanding TiO_2 nanotube arrays on FTO substrate as photoanode, Mater. Chem. Phys. 125 (2011) 612–616.
[21] K.-L. Li, Z.-B. Xie, S. Adams, A reliable TiO_2 nanotube membrane transfer method and its application in photovoltaic devices, Electrochim. Acta 62 (2012) 116–123.
[22] P. Roy, D. Kim, I. Paramasivam, P. Schmuki, Improved efficiency of TiO_2 nanotubes in dye sensitized solar cells by decoration with TiO_2 nanoparticles, Electrochem. Commun. 11 (2009) 1001–1004.
[23] O.K. Varghese, M. Paulose, C.A. Grimes, Long vertically aligned titania nanotubes on transparent conducting oxide for highly efficient solar cell, Nat. Nanotechnol. 4 (2009) 592–597.
[24] S. Kathirvel, C. Su, C.-Y. Yang, Y.-J. Shiao, B.-R. Chen, W.-R. Li, The growth of TiO_2 nanotubes from sputter-deposited Ti film on transparent conducting glass for photovoltaic applications, Vacuum 118 (2015) 17–25.
[25] P. Chen, J. Brillet, H. Bala, P. Wang, S.M. Zakeeruddin, M. Grätzel, Solid-state dye-sensitized solar cells using TiO_2 nanotube arrays on FTO glass, J. Mater. Chem. 19 (2009) 5325–5328.
[26] C. Grätzel, S.M. Zakeeruddin, Recent trends in mesoscopic solar cells based on molecular and nanopigment light harvesters, Mater. Today 16 (2013) 11–18.
[27] J. Dervaux, P.-A. Cormier, S. Konstantinidis, R. Di Ciuccio, O. Coulembier, P. Dubois, R. Snyders, Deposition of porous titanium oxide thin films as anode material for dye sensitized solar cells, Vacuum 114 (2015) 213–220.
[28] G.K. Mor, O.K. Varghese, M. Paulose, C.A. Grimes, Transparent highly ordered TiO_2 nanotube arrays via anodization of titanium thin films, Adv. Funct. Mater. 15 (2005) 1291–1296.
[29] A.-F. Kanta, M. Poelman, A. Decroly, Electrochemical characterisation of TiO_2 nanotube array photoanodes for dye-sensitized solar cell application, Sol. Energy Mater. Sol. Cells 133 (2015) 76–81.
[30] S.P. Albu, P. Schmuki, Influence of anodization parameters on the expansion factor of TiO_2 nanotubes, Electrochim. Acta 91 (2013) 90–95.
[31] D. Regonini, A. Satkab, A. Jaroenworaluck, D. Allsopp, C. Bowen, R. Stevens, Factors influencing surface morphology of anodized TiO_2 nanotubes, Electrochim. Acta 74 (2012) 244–253.
[32] H. Zheng, A.Z. Sadek, M. Breedon, D. Yao, K. Latham, J. du Plessis, K. Kalantar-Zadeh, Fast formation of thick and transparent titania nanotubular films from sputtered Ti, Electrochem. Commun. 11 (2009) 1308–1311.
[33] J. Manifacier, J. Gasiot, J. Fillard, A simple method for the determination of the optical constants n, h and the thickness of a weakly absorbing thin film, J. Phys. E Sci. Instrum. 9 (1976) 1002–1004.
[34] F. Fabregat-Santiago, G. Garcia-Belmonte, I. Mora-Sero, J. Bisquert, Characterization of nanostructured hybrid and organic solar cells by impedance spectroscopy, Phys. Chem. Chem. Phys. 13 (2011) 9083–9118.
[35] J. Bisquert, Influence of the boundaries in the impedance of porous film electrodes, Phys. Chem. Chem. Phys. 2 (2000) 4185–4192.
[36] I. Abayev, A. Zaban, F. Fabregat-Santiago, J. Bisquert, Electronic conductivity in nanostructured TiO_2 films permeated with electrolyte, Phys. Status Solidi A 1 (2003) R4–R6.